Bachelor Thesis

Study of Efficiencies of $B^0 \to K^+\pi^- l^+ l^-$ and $B^0 \to K^+\pi^-\ J/\psi(\to l^+ l^-)$ at LHCb

by

Andrej Isaac Maraffio

Supervisors:

Dr. Patrick Owen

Dr. Rafael Silva Coutinho

Jonas Eschle

Supervising Professor:

Prof. Dr. Nicola Serra

April 2023

"Ci sono soltanto due possibili conclusioni: se il risultato conferma le ipotesi, allora hai appena fatto una misura; se il risultato è contrario alle ipotesi, allora hai fatto una scoperta."

-Enrico Fermi

Mathematisch-naturwissenschaftliche Fakultät der

Universität Zürich[UZH]

Abstract

Faculty of Science

Physics Institute

Apart from mass variations, the three charged leptons in the Standard Model are exact copies of one another, and the electroweak coupling of the gauge bosons to leptons is independent of lepton flavor. This hypothesis is known as lepton flavor universality (LFU) and has been thoroughly investigated. Any violation of LFU in tree level decays would be a clear indicator of physics beyond the Standard Model. New Physics particles that preferentially link to the 2nd and 3rd generations of leptons are very susceptible to experimental testing of LFU in semileptonic b-hadrons or uncommon b decays.
The purpose of this study is to figure out how the efficiencies of the rare and resonant decay behave.

Acknowledgements

First of all, I want to thank Dr. Prof. Serra for giving me the opportunity to do my Bachelor's thesis in his group. This thesis has given me the opportunity to gain and pass on an insight into today's research at CERN.

I would also like to thank Dr. Patrick Owen for our weekly meetings, for showing me the way through the analysis and finally for always being available for questions.

Further I want to thank Dr. Rafael Silva Coutinho for his help at the beginning of my work when I was having difficulties with the Python script.

Another thank you goes to Jonas Eschle for his help when I had technical problems with my computer and for his support in writing my thesis.

And finally a big thank you goes to my parents for their financial and motivational support throughout my studies!

Table of Contents

Chapter 1

Introduction

1.1 Standard Model

In the so-called Standard Model (SM) of particle physics, physicists have summarized their understanding of the tiniest particles and their interactions. With the exception of the gravitational force, it accurately represents all of the phenomena of the microcosm that we are aware of, namely the matter particles and the forces operating between them. The Higgs boson, which is another component of the SM, is a Higgs-field excitation that, simplified, is accountable for the reason that the other elementary particles have mass.

The interactions or forces that keep matter together are interactions or forces between the particles of matter. The world around us would collapse into its tiny components if this were not the case. The electromagnetic force, the weak force, and the strong force are the interactions. They emerge as a result of the interchange of so-called gauge bosons between matter particles. Gravity, the fourth known fundamental force, has no effect in the microcosm. Photons are exchanged to form the electromagnetic force, which works across extremely long distances between charged particles, because of the photon being massless. Inside protons and neutrons, the strong force maintains the quarks together. The matter particles interchange gluons, which come in eight distinct varieties and have an effective range of just the atomic nucleus. All elementary particles, even those that are not electrically charged, are affected by the weak force. The weak force happens via the interaction of Z and W bosons and has a limited range, due to the enormous masses of the exchange particles that mediate it. The W and Z bosons are over 100 times heavier than a proton.

There are a total of twelve matter particles, the so called fermions (particles with spin 1/2), split into six quarks and six leptons. Both groupings are made up of particles

from three different generations. Each generation is made up of two quarks and two leptons, which are known as flavours. The characteristics of the particles in the various generations are identical, but their mass differs: matter particles in the second and third generation are heavier than those in the first.

Generation	**I**	**II**	**III**
Quarks	$\begin{pmatrix} u \\ d \end{pmatrix}$	$\begin{pmatrix} c \\ s \end{pmatrix}$	$\begin{pmatrix} t \\ b \end{pmatrix}$
Leptons	$\begin{pmatrix} \nu_e \\ e^- \end{pmatrix}$	$\begin{pmatrix} \nu_\mu \\ \mu^- \end{pmatrix}$	$\begin{pmatrix} \nu_\tau \\ \tau^- \end{pmatrix}$

Furthermore, the second and third generations' elementary particles are unstable, decaying into particles from the first generation. Quarks are the constituents of hundreds of composite particles, amongst them the only two stable ones protons and neutrons, which make up the atomic nucleus. The electrical charge of the 'up-type' quarks (u, c, t) is $+2/3$, whereas that of the 'down-type' quarks (d, s, b) is $-1/3$. Charged (e^-, μ^-, τ^-) and uncharged $(\nu_e, \nu_\mu, \nu_\tau)$ leptons are the two types of leptons that exist. The first type has an electrical charge of -1, whereas the second type is uncharged and is appropriately named neutrino.

1.2 Lepton Flavor Universality

The three charged lepton flavors in the Standard Model are identical, aside from their mass. The gauge bosons mediating the weak interaction have an identical couplings to the three lepton flavors. Therefore, leptonic decays involving the weak interaction should also have comparable branching ratios for the various families. This phenomenon is also known as the Lepton Flavor Universality (LFU). Any violation of this universality would be a signal for New Physics (NP) beyond the SM. The semileptonic decays of heavy hadrons, of all three generations, offer a great laboratory for testing LFU. Many models that extend the SM include extra interactions that potentially violate the LFU.
Physics beyond the SM with LFU violation expect different couplings for different generations, which means that this is ideally adapted to search for LFU violation. A single vertex, according to the SM, may only alter a particle's flavor from up-type to down-type or vice versa. Therefore, there are no Flavour Changing Neutral Currents (FCNC). In other words, according to the SM, there are no processes, where the flavor of the quark is changed without a change in the electric charge. As seen on the left side of Fig. 1.1, these FCNC must pass through amplitudes using electroweak loop diagrams, also known as Penguin diagrams and do not occure on tree level.

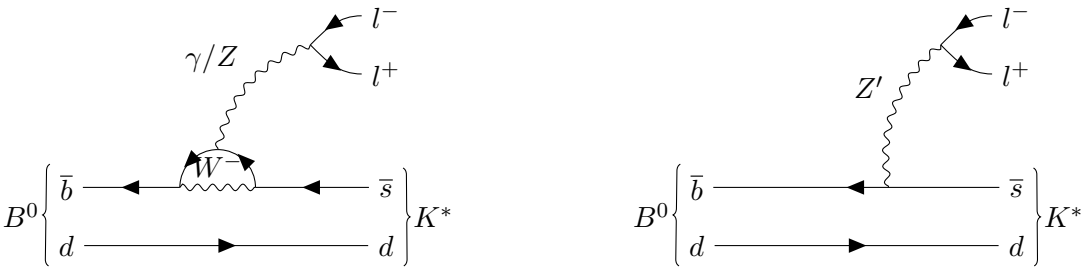

FIGURE 1.1: Penguin Diagram of the $B^0 \to K^* \ell^+ \ell^-$ decay and a possible NP contribution with a new particle Z'

Since the beginning of the LHCb experiment, studies of decays mediated by the FCNC, such as $B^0 \to K^* \ell^+ \ell^-$ and others, have been analyzed.

According to current study [1], the ratio of electronic and muonic decay rates, shown in equation 1.1, is significantly different from unity, indicating that the B_0 has a higher likelihood of decaying into an electron-positron pair than its muonic counterpart, breaking LFU. In other words these results are an indicator for new physics.

$$R_{K^*} = \frac{\mathcal{B}\left(B^0 \to K^* \mu^+ \mu^-\right)}{\mathcal{B}\left(B^0 \to K^* e^+ e^-\right)} \tag{1.1}$$

To calculate the R_{K^*} value we have to take many things into account, since electrons and muons behave differently in the detector, especially in terms of detection efficiency. The branching ratios are normalised with those of the resonant mode J/ψ, which reduces experimental systematic errors. In the analysis we looked at the following ratio:

$$R_{K^*} = \frac{\mathcal{B}\left(B^0 \to K^* \mu^+ \mu^-\right)}{\mathcal{B}\left(B^0 \to K^* J/\psi\left(\to \mu^+ \mu^-\right)\right)} \Big/ \frac{\mathcal{B}\left(B^0 \to K^* e^+ e^-\right)}{\mathcal{B}\left(B^0 \to K^* J/\psi\left(\to e^+ e^-\right)\right)} \tag{1.2}$$

The resonant channels containing the decay $J/\psi \to \ell^+ \ell^-$ are found to be compatible with LFU, i.e. the ratio $\mathcal{B}\left(J/\psi \to e^+ e^-\right) / \mathcal{B}\left(J/\psi \to \mu^+ \mu^-\right)$ is found to be compatible with unity, so the double ratio may be investigated rather than the single ratio. Because the resonant and non-resonant decays have comparable experimental signatures, systematic effects are reduced, and the ratio's uncertainty is ultimately dominated by statistical uncertainty.

This resonant channel's ratio also serves as a cross-check, verifying that the differences in experimental signatures for muons and electrons are well understood and accounted for.

1.2.1 Known Branching Fractions

In lepton flavour non-universal observables R_K and R_{K^*}, the LHCb experiment recently discovered signs of new physics (NP).
R_K and R_{K^*} have been measured in the dilepton invariant mass squared, $q^2 \in [1{-}6]GeV^2$, where the measured R values are as follows [2] [3]:

$$R_K = 0.86 \pm 0.06$$

$$R_{K^*} = 0.68 \pm 0.18$$

The deviations from the Standard Model (SM) are only at the level of 3.1σ respectively 2.2σ. $B^0 \to (K \text{ or } K^*)\, l^+l^-$ decays are proceed through $b \to s$ flavour changing neutral current (FCNC) transitions at the quark level.
The individual branching ratios $\mathcal{B}\left(B^0 \to K^*\mu^+\mu^-\right)$ and $\mathcal{B}\left(B^0 \to K^*e^+e^-\right)$ are predicted with comparatively larger hadronic uncertainties in the SM.

1.3 Goal of the Analysis

When the same cuts are applied to both samples corresponding to data collected over the same moment, the branching fraction should be very similar (up to a permille) [4].
The purpose of this study was to compare the branching ratios of the following decays:

- $B^0 \to K^+\pi^-e^+e^-$
- $B^0 \to K^+\pi^-\mu^+\mu^-$
- $B^0 \to K^+\pi^-J/\psi\,(\to e^+e^-)$
- $B^0 \to K^+\pi^-J/\psi\,(\to \mu^+\mu^-)$

In other words we compare the decays $B^0 \to K^+\pi^-l^+l^-$ to those of $B^0 \to K^+\pi^-\ J/\psi(\to l^+l^-)$, where the J/ψ decays into two electrons or muons.
Analogous to Eq. 1.2, the aim of the analysis is to measure the fraction of the following branching fractions.

$$R_{K^+\pi^-} = \frac{\frac{\mathcal{B}\left(B^0\to K^+\pi^-\mu^+\mu^-\right)}{\mathcal{B}(B^0\to K^+\pi^-e^+e^-)}}{\frac{\mathcal{B}(B^0\to J/\psi(\to\mu^+\mu^-)}{\mathcal{B}(B^0\to J/\psi(\to e^+e^-)}} \tag{1.3}$$

Since $B^0 \to K^+\pi^-\ J/\psi(\to l^+l^-)$ has the same final state as $B^0 \to K^+\pi^-l^+l^-$ and since its branching ratio is very well measured, we can use this decay as a control channel as mentioned before.

The branching fractions ratio is calculated by using the number of events found by the fits, normalised to the efficiency ratio:

$$\frac{\mathcal{B}\left(B^0 \to K^+\pi^-\mu^+\mu^-\right)}{\mathcal{B}\left(B^0 \to K^+\pi^-e^+e^-\right)} = \frac{\mathrm{Nsig}_{B^0\to K^+\pi^-\mu^+\mu^-}}{\mathrm{Nsig}_{B^0\to K^+\pi^-e^+e^-}} \cdot \frac{\epsilon_{B^0\to K^+\pi^-e^+e^-}}{\epsilon_{B^0\to K^+\pi^-\mu^+\mu^-}} \tag{1.4}$$

We are, however, interested in the double ratio, as shown in equation 1.3, which can be rewritten in the same way as formula 1.4 was.
As a result, we have:

$$\frac{\frac{\mathcal{B}\left(B^0\to K^+\pi^-\mu^+\mu^-\right)}{\mathcal{B}(B^0\to K^+\pi^-e^+e^-)}}{\frac{\mathcal{B}(B^0\to J/\psi(\to\mu^+\mu^-)}{\mathcal{B}(B^0\to J/\psi(\to e^+e^-)}} = \frac{\frac{\mathrm{Nsig}_{B^0\to K^+\pi^-\mu^+\mu^-}}{\mathrm{Nsig}_{B^0\to K^+\pi^-e^+e^-}} \cdot \frac{\epsilon_{B^0\to K^+\pi^-e^+e^-}}{\epsilon_{B^0\to K^+\pi^-\mu^+\mu^-}}}{\frac{\mathrm{Nsig}_{B^0\to K^+\pi^-\ J/\psi(\to\mu^+\mu^-)}}{\mathrm{Nsig}_{B^0\to K^+\pi^-\ J/\psi(\to e^+e^-)}} \cdot \frac{\epsilon_{B^0\to K^+\pi^-\ J/\psi(\to e^+e^-)}}{\epsilon_{B^0\to K^+\pi^-\ J/\psi(\to\mu^+\mu^-)}}} \tag{1.5}$$

This equation will play an important role in the analysis in Chapter 5.

Chapter 2

Large Hadron Colider

The Large Hadron Collider (LHC) [5] has been the most powerful particle accelerator ever constructed and the newest addition to the CERN accelerator complex since its inauguration on September 10, 2008, when the first beam successfully completed a round trip [6]. The LHC is housed in an underground tunel with an average depth of $100m$ near the Swiss-French border.

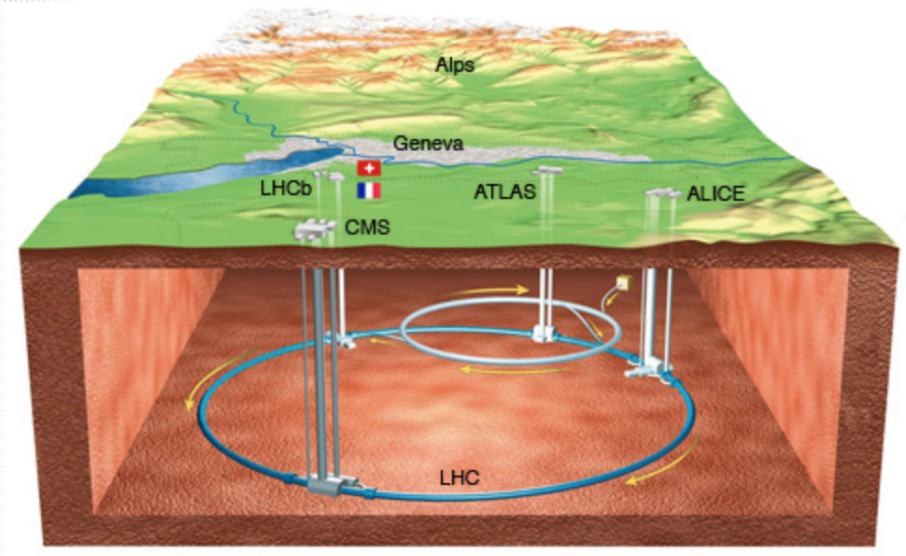

FIGURE 2.1: CERN's Large Hadron Collider [7].

The LHC uses superconducting magnets cooled to -271.3°C to accelerate two proton beams in opposing directions. They travel in groupings (bunches) through pipes that are maintained at ultrahigh vacuum pressures ranging from $1 \cdot 10^{-7}$ to $10^{-9} Pa$ [8]. Protons reach speeds of 99.9999% c and will ultimately collide with other protons, producing a variety of particles called collision debris.

Protons are produced by removing electrons from hydrogen atoms held in a tiny hydrogen bottle. The particles are then sent through a series of increasing-energy pre-accelerators before being injected into the LHC ring. The pre-accelerators have energies of up to 50 MeV for the Linear Accelerator 2 (LINAC2), 1.4 GeV for the Proton Synchrotron Booster (PSB), 25 GeV for the Proton Synchrotron (PS), and 450 GeV for the Super Proton Synchrotron (SPS).

2.1 Main detectors

The beams that go through the LHC are accelerated, twisted, and focussed by particular magnet arrays, which also compress them seconds before they meet. These collisions take place at four distinct Interaction Points (IPs) throughout the ring, which correspond to the four large particle detectors: ATLAS, CMS, ALICE, and LHCb.

2.1.1 Atlas

ATLAS (A Toroidal LHC Apparatus) is the biggest of the four detectors and one of the two general-purpose detectors. It is 46 meters in length, 25 meters in diameter, and weighs 7000 tons. ATLAS and CMS reported in collaboration the discovery of the Higgs boson [10] in July 2012. Figure 2.2 shows a schematic of the ATLAS detector.

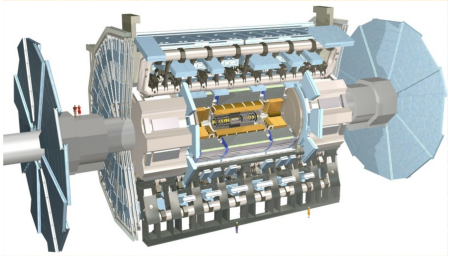

FIGURE 2.2: ATLAS detector [9].

2.1.2 CMS

CMS (Compact Muon Solenoid) is a general-purpose detector that is based on a solenoidal superconducting magnet that produces a 4 Tesla magnetic field and weighs roughly 12000 tonnes. It measures 21 meters in length, 15 meters in width, and 15 meters in height [12]. Figure 2.3 shows a schematic view of the CMS detector.

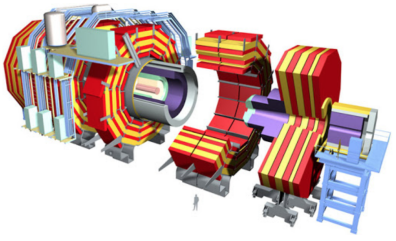

FIGURE 2.3: CMS detector [11].

2.1.3 Alice

ALICE (A Large Ion Collider Experiment) is devoted to heavy ion collisions, allowing for the study of quark-gluon plasma, which is of special relevance in QCD research [14]. Figure 2.4 shows a schematic view of the ALICE detector.

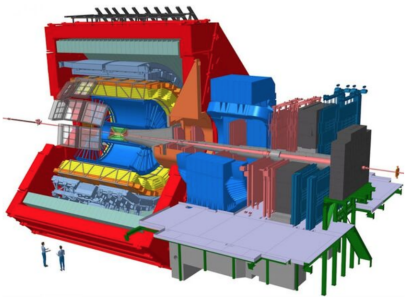

FIGURE 2.4: ALICE detector [13].

2.1.4 LHCb

The LHCb (LHC-beauty) experiment focuses on the matter-antimatter asymmetry in b quarks [16]. Figure 3.1 shows a schematic of the LHCb detector. We will take a closer look at this detector in the next chapter.

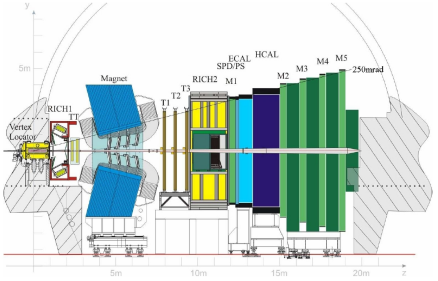

FIGURE 2.5: LHCb detector [15].

Chapter 3

LHCb

The main goal of the LHCb experiment (Large Hadron Collider Beauty) is to measure B decays and muons. The probing of the SM is done in an indirect way by studying CP violation and rare decays of heavy hadrons. It is also known as heavy flavour physics, which is the study of the properties and decays of these heavy particles that include beauty (b) and/or charm (c) quarks generated in proton-proton collisions at the LHC. In such rare decays a d quark and a $\bar{b}$ antiquark are created in parallel.
When a $b\bar{b}$ quark pair is created in the direction of the beam axis, the associated particle is most likely to travel in the same direction. This explains the geometry of the LHCb detector, which is constructed as a forward spectrometer with a polar angular coverage ranging from 10 to 300 milliradians ($mrad$) in the horizontal plane and 250 milliradians ($mrad$) in the vertical plane. Only one of the two available orientations is instrumented due to financial reasons.

The LHCb detector, like all other LHC detectors, provides a beam conditions monitor (BCM). Diamond sensors located near the beam axis are used by the BCM to monitor the beam quality. As charged particles travel through the sensors, the ionisation caused by them is measured. The beam in the LHC is automatically directed out of the accelerator and disposed of (beam dump) if the signal exceeds certain thresholds, protecting the detector from damage caused by "out-of-control" beams.

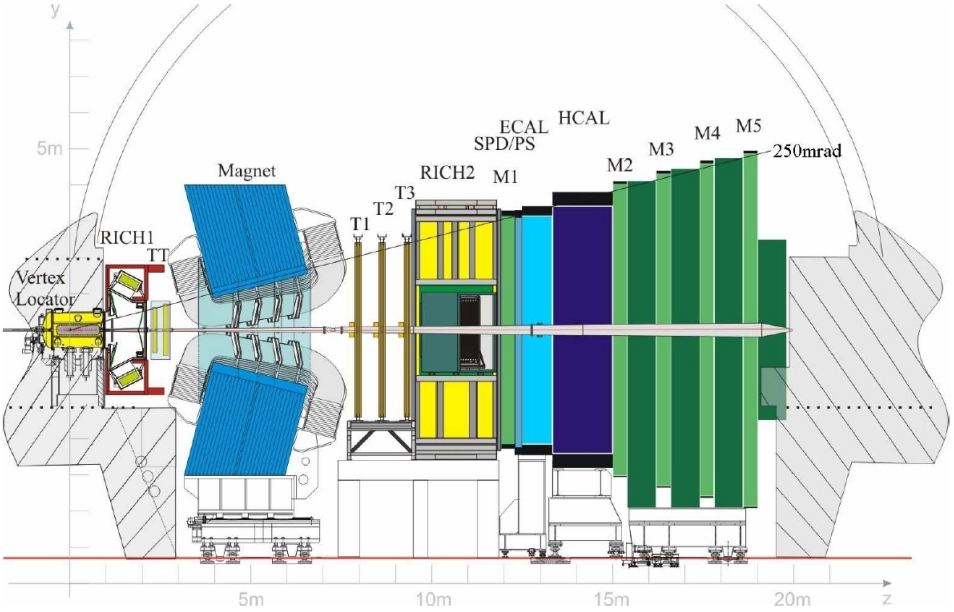

FIGURE 3.1: LHCb Detector [15]

Each of the LHCb's sub-detectors is focused on a distinct aspect of the particles created by colliding protons. The detector's components work together to collect data on the identity, trajectory, momentum, and energy of each particle produced, allowing them to identify individual particles among the billions that scatter out from the impact site.

3.1 Vertex Locator (VELO)

The VELO sub-detector is the only place where the LHC proton beams collide and particles containing b and anti-b quarks are created. The VELO's goal is to find B mesons, which is a nontrivial task. The difficulty comes from the fact that these B-mesons only survive for 10^{-12} of a second and travel only over one millimetre before decaying into other particles. The second reason is that they spend their brief existence close to the beam, and in order to detect them, the VELO sub-detector must be placed near the LHC beam, since it was built to perform precise measurement of their decay positions. The VELO uses a revolutionary design feature to protect itself from the LHC proton beams, while the beams are being injected and stabilized, the silicon elements are kept out of harm's way, but once safe, they are mechanically brought in towards the beam to search for B particles.

The VELO sub-detector is made up of two rows of 42 half-moon-shaped silicon sensors, each 0.3 mm thick and with a tiny cutout in the middle that allows the main LHC beam to pass through undisturbed when the detector is just seven millimeters away.

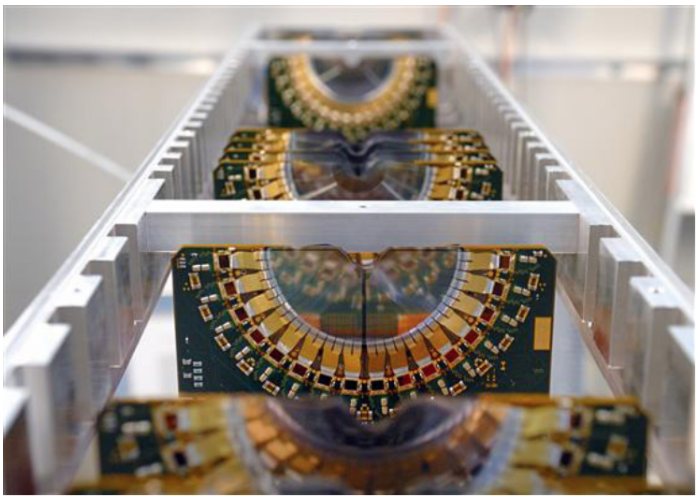

FIGURE 3.2: VELO Sub-Detector

The VELO monitors the distance between where protons collide - and B particles are generated - and where the B particles decay into multiple particles that VELO can detect. As a result, the B particles are never explicitly detected; their existence is deduced from the distance between these two places. In summary, VELO can identify the location of B particles to within 10 microns (100th of a millimetre).

3.2 Ring Imaging Cherenkov (RICH)

The experiment's two RICH detectors are designed for particle identification, with the goal of detecting charged particles (including pions, kaons, and protons) with a momentum of 1-150 GeV/c and an angular acceptance of 10-300 milliradians (mrad). The two detectors, which are located on opposite sides of the LHCb's strong magnet, detect particles traveling at different speeds and angles. The RICH work by detecting Cherenkov radiation emissions.

Cherenkov radiation is electromagnetic radiation emitted when a charged particle travels faster through a dielectric media than the phase velocity (speed of propagation of a wavefront in a medium) of light. This phenomenon is comparable to the cone which an aircraft creates by breaking the sound barrier.

The particle emits a cone of light when its travel, which the RICH detectors reflect onto an array of sensors by using mirrors. The form of the light cone is determined by the particle's velocity, allowing the detector to calculate the particle's speed. With this information and a record of its trajectory (collected using the tracking system and a magnetic field) the particles mass and charge can be calculated and therefore also its identity.

3.3 Trackers

The tracking system's main goal is to reconstruct charged-particle paths as quickly and precisely as possible. When charged particles, such as electrons and protons, move through particular substances, they leave behind trails that the trackers can detect. These are used in RICH detectors to reconstruct Cherenkov rings. They allow the track of each particle traveling through the detector to be recorded, which helps in the linking of the signals left in the other detector elements and is essential for reconstructing B particle decays.
The main LHCb tracking system consists of four stations: one ("TT") is placed between RICH-1 and the LHCb dipole magnet, while the other three ("T1-T3) are over 3 meters between the magnet and RICH-2.
Each of these four LHCb tracking systems covers an area of about 40 m2 and incorporates two separate detector technologies.
The silicon tracker, which is close to the beam pipe, detects passing particles using silicon microstrip detectors. When charged particles hit with silicon atoms, electrons are liberated, and an electric current is created, indicating the original particle's path.
The outer tracker is made up of hundreds of gas-filled straw tubes and is located further away from the beam pipe. When a charged particle passes through, gas molecules are ionized and electrons are produced. The track's location is determined by measuring the time it takes electrons to reach an anode wire in the tube's center.

3.4 Calorimeter

The calorimeter system is meant to fully stop particles as they travel through the detector, allowing to calculate the amount of energy lost when each one comes to a halt.
At LHCb, two types of calorimeters are used.
The experiment's electromagnetic calorimeter (ECAL) measures the energy of lighter particles like electrons and photons, while the hadron calorimeter (HCAL) measures the energy of protons, neutrons, and other quark-containing particles. The construction of both calorimeters is made up of alternating layers of metal and plastic plates. When particles collide with metal plates, they create secondary particle showers. These, in turn, stimulate polystyrene molecules inside the plastic plates, causing UV light to be emitted. The energy of the particles entering the calorimeter determines how much UV is generated.
Calorimeters are the most common technique of recognizing non-electrically charged particles like photons and neutrons.

3.5 Muon System

Muon triggering and offline muon identification are fundamental parts of the LHCb experiment. Muons are present in the final states of many CP-sensitive B decays and play an important part in CP asymmetry and oscillation studies, since muons from semi-leptonic b decays offer a tag of the accompanying neutral B mesons' starting state flavour. The system, which is located at the detector's far end, is made up of five rectangular stations (M1-M5) that span an acceptance range of 300 mrad horizontally and 250 mrad vertically. M1 is placed in front of the pre-shower/scintillating pad detector. M2-M5 are separated by iron filters and following the hadron calorimeter (HCAL). The stations take up 435 m2 of space. Each station has chambers which are filled with a mixture of carbon dioxide, argon, and tetrafluoromethane. The muons traveling through react with the mixture, and the effects are detected by wire electrodes. The muon system has around 1,400 chambers and 2.5 million wires in total.

3.6 The Magnet

The massive magnet for the experiment is made up of two 27-tonne coils installed within a 1,450-tonne steel frame. Each coil is made up of ten 'pancakes,' each wound with about 3,000 meters of aluminum wire. The Lorenz force causes the trajectories of charged particles to be bent in the presence of a magnetic field, with positive and negative particles experiencing forces in opposing directions. It is possible to compute with a particle's momentum in combination with v (from RICH) its identity by looking at the curvature of the route.

3.7 Trigger

When LHCb is fully functional, the detector is expected to record 10 million proton collisions per second. This implies that at the interaction point, proton bunches interact at a rate of 40 MHz, making it difficult to capture all of these 'events' on a limited storage capacity. LHCb uses an electrical technology known as a 'trigger' to choose the best of them. The LHCb trigger system involves two phases of operation. The Level-0 trigger reduces the rate to 1MHz and is used in custom electronics. It makes use of the fact that particles produced by a B decay have a larger transverse momentum in respect to the particle beam axis (pT) than particles produced by the main proton-proton interaction. L0 uses calorimeters and the muon system, which are sub-detectors capable of selecting high-pT particles at the required high rate. Furthermore, it employs the VELO's two

specialized silicon layers to perform a simplified vertex reconstruction, allowing events with multiple proton-proton interactions to be rejected, which is particularly challenging to reconstruct and evaluate in B meson decays.
The HLT algorithm is executed on a farm of 1000 16-core machines with full access to detector data. It is separated into two sub-levels: HLT1, which produces a few tens of kHz, and HLT2, which gives the recorded 2kHz.

3.7.1 Trigger decision category: TIS, TOS and TISTOS

An event may be categorised into three non-exclusive categories at any level of the trigger:

- Trigger On Signal (TOS): Events that are triggered by a signal decay independent of whether the rest of the event is present. If there is at least one trigger object with all of its tracks overlapping with the signal, the TOS requirement is fulfilled.
- Trigger Independent of Signal (TIS): Events take place independently whether or not the signal is present. There must be at least one trigger object that does not overlap with the signal in order for such event to be TIS. Except for correlations between the signal decay and the rest of the event, TIS events are trigger unbiased.
- Trigger Decision (TISTOS): Events triggered by either a signal trigger (TOS) or a trigger independent of the signal (TIS) without distinguishing between the two.

Chapter 4

Dataset

In this analysis, data generated by Monte Carlo simulations were used to simulate the data from LHCb measured during 2016.

The decays, which were mentioned in Chapter 1 Introduction, were considered, because they are believed to provide a clue to the physics behind the standard model. The first two decays are the so-called rare decays and the others are the resonant decays.

4.1 Monte Carlo Simulation

Monte Carlo simulation is used in all phases of experimental particle physics, including the investigation of detector concepts' physics reach, the design of facilities and detectors, the development and optimization of data reconstruction software, and data analysis for the generation of physics results. These pp collisions are created by PYTHIA [17] and the decay and time evolution are created by the event generator EvtGen [18]. The LHCb simulation application [19], Gauss, uses these two phases to create the simulated events, which then are used almost the same as the real data.

4.1.1 PYTHIA

PYTHIA is a typical instrument for generating high-energy collisions, consisting of a coherent collection of physics models for the development from a few-body to a complicated multihadronic end state. It includes a library of processes and models for parton showers in the early and final states, multiple parton-parton interactions, beam remnants, string fragmentation and particle decay.

4.1.2 EvtGen

The EvtGen package offers a framework for implementing physics processes related to B meson decays and other resonant decays. A detailed decay table for B decays, models of time dependent CP asymmetries in neutral B meson decays and semileptonic form-factor models are just a few of the incorporated features.

4.1.3 LHCb simulation, Gauss

Gauss, the LHCb simulation tool, consists of two phases, the creation of the primary event and the tracking of particles. The first phase can be broken into two primary parts, which both need external generator packages. The first is particle creation from the LHC beams' initial pp collision, which is implemented by the event generator PYTHIA. Secondly, the decay and time evolution of the produced particles using mainly the EvtGen package. Gauss, the simulation software, is connected to these two external generators and offers the essential algorithms for steering the execution of the various generation sequences and ensuring their coherence. The combined software is flexible enough to produce a wide range of events, from common B meson decays to very unusual ones.

Chapter 5

Analysis

5.1 Electron efficiency

As mentioned in Chapter 1 Introduction in the equation 1.5, the ratio between the efficiencies are crucial parts of the measurement of the ratio of the branching fractions. Therefore, the ratio of the efficiencies of the rare and resonant decay with e^-e^+ in the final state was investigated in this work.
The following efficiencies are always calculated by dividing the events after the cut by the events before the cut, denoted as $\epsilon = \frac{n_{\text{after cut}}}{n_{\text{before cut}}}$. This means that the following ratio was considered:

$$\frac{\epsilon_{B^0 \to K^+\pi^- e^+e^-}}{\epsilon_{B^0 \to K^+\pi^-\ J/\psi(\to e^+e^-)}} \tag{5.1}$$

All the efficiencies were calculated in dependence of different variables, in our case, total momentum P and the transverse momentum PT for the B-meson and the lepton.
In addition, there are also the TIS and TOS conditions. The TOS condition means that the signal electron fired the trigger and the TIS condition, on the other hand, means that something else of the whole event fired the trigger.
The results of these efficiencies are listed in the table 5.1.

Trigger (Variables in bin)	$\epsilon_{K^+\pi^- e^+e^-}$	$\epsilon_{K^+\pi^- J/\psi(\to e^+e^-)}$	$\epsilon_{K^+\pi^- J/\psi(\to e^+e^-)}$ *to* $\epsilon_{K^+\pi^- e^+e^-}$
TIS (B_P)	31.572 ± 0.567	29.700 ± 0.069	30.154 ± 0.163
TIS (B_PT)	31.572 ± 0.567	29.702 ± 0.069	30.103 ± 0.163
TOS (max_L_P)	42.367 ± 0.533	50.771 ± 0.063	44.602 ± 0.144
TOS (max_L_PT)	42.367 ± 0.533	50.771 ± 0.063	39.492 ± 0.144

TABLE 5.1: Tabel of efficency for different variables in [%].
In the last column the translation from $\epsilon_{K^+\pi^- J/\psi(\to e^+e^-)}$ to $\epsilon_{K^+\pi^- e^+e^-}$.

The uncertainty on these efficiencies ϵ was obtained with the formula $\sigma_\varepsilon = \frac{\sqrt{n_{\text{after cut}}(1-\varepsilon)}}{n_{\text{before cut}}}$, where for this calculation the efficiency is the estimated efficiency. To get a more precise overview of how these efficiencies behave, we plot them. The aim is to see how they differ from each other for the different variables.
These results are shown in figure 5.1.

As previously mentioned, the goal of this project is to study the different correlations of the rare and resonant decay by dividing the two efficiencies as shown in equation 5.1. One can thus see how the efficiencies change according to the variables, allowing to obtain further conclusions as a result of this.
The efficiency of the fraction of the rare and the resonant decay are calculated using the formula 5.1. The error on this fraction was calculated by summing the errors of the two decays and then dividing it by the estimated efficiency.
The results are shown in table 5.2.

Conditions	$\frac{\epsilon_{B^0\to K^+\pi^-e^+e^-}}{\epsilon_{B^0\to K^+\pi^- J/\psi(\to e^+e^-)}}$
TIS_B_P	1.062 ± 0.022
TIS_B_PT	1.063 ± 0.022
TOS_max_L_P	0.835 ± 0.012
TOS_max_L_PT	0.834 ± 0.012

TABLE 5.2: Division of the rare decay mode by the resonant decay mode

5.2 Interpretation

The efficiency of the resonant decay translated to the efficiency of the rare decay, as shown in table 5.1, is of central importance to us. For the TIS condition, the efficiencies are quite similar, as also the translation from resonant to rare decay. The situation is quite different for the TOS condition.
The reason for this is, that with the Trigger Independent Signal (TIS), something else from the event (not the leptons) has fired the trigger. Thus, we expect a similar efficiency for the two decays.
With the Trigger On Signal (TOS), however, we consider e^-e^+ with maximum momentum and maximum transverse momentum. This means that we also expect a higher efficiency in resonant decay, because a J/ψ is created first, which has a higher mass/energy than the rare decay, which decays direct into the two leptons.
Moreover, this interpretation is also confirmed in Table 5.2.

Furthermore, we can say, that for TOS and TIS conditions, different variables are more correlated than others.
In TOS, for example, the variable L_P and L_PT are strongly correlated, since we concentrate here on the end product, namely the leptons. With TIS, on the other hand, no correlation is expected, as it is independent of the signal. However, we still excect this to be correlated, because when two protons collide, a gluon is formed which then produces a pair of b and $\bar{b}$. In the process, b and $\bar{b}$ couple to the u and $\bar{u}$ quark and produce B and $\bar{B}$ Meson. Due to the conservation laws for the B meson, the variables of B_P and B_PT are of central importance here.

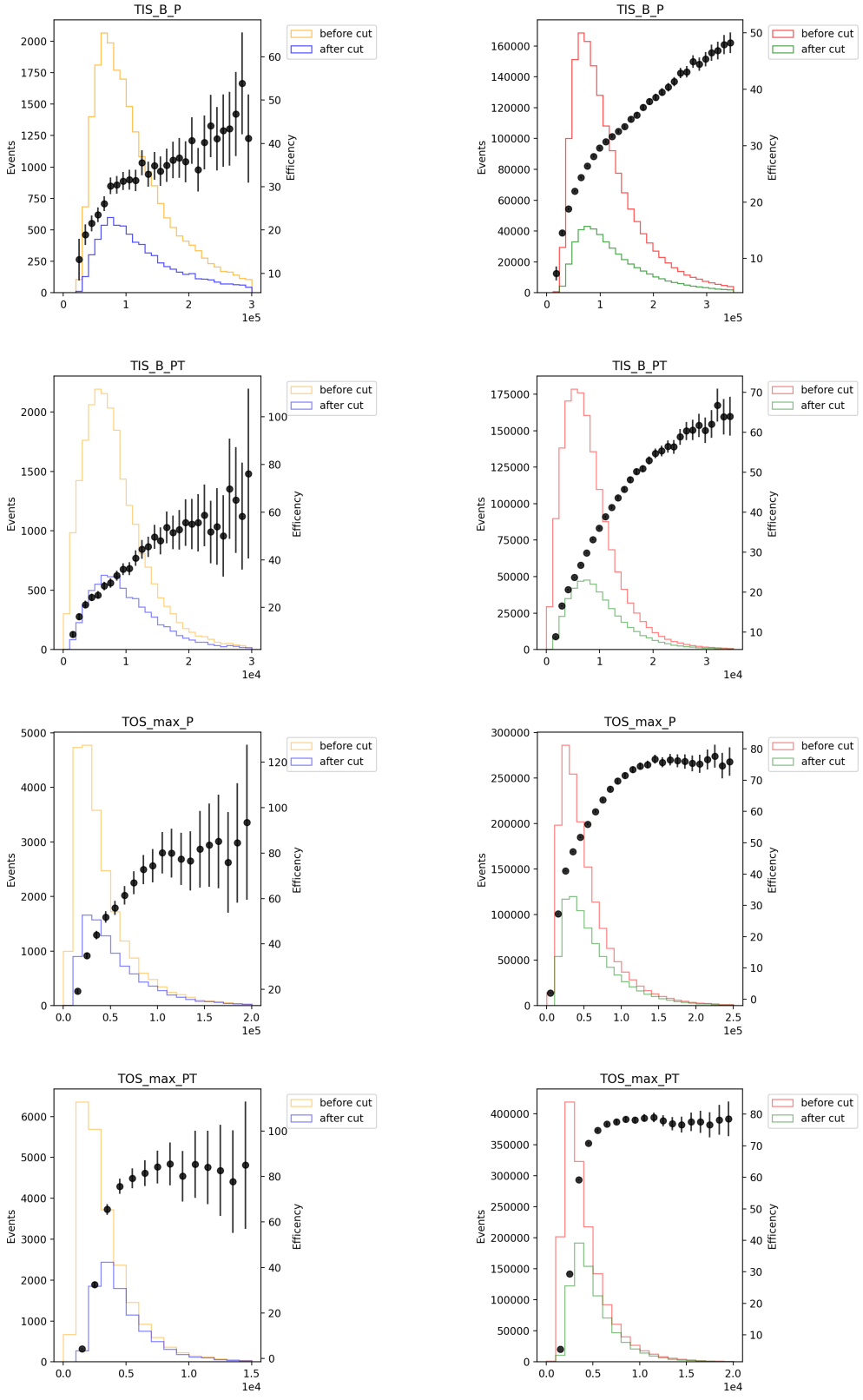

FIGURE 5.1: Efficiency for different variables.
In this figure we have the rare decay on the left and resonant decay on the right side. The importance of these plots is to see the trend of the individual efficiencies for the different variables.

Chapter 6

Conclusion

The goal in this work was to understand the efficiencies of the two, rare and resonant, decay modes in different cuts and their differential efficiencies in certain kinematic variables. This understanding is crucial in order to calculate the branching fraction of each decay individually as well as the ratio of the rare and resonant decay mode as shown in equation 1.4.
The work consisted mainly of calculating the efficiencies shown in Table 5.1.
Then, in a second step, the efficiency of the resonant decay translate to the efficiency of the rare decay, where the results can be seen in the third column of Table 5.1.
The next step was to plot the individual efficiencies differential in the variables listed in Table 5.1 to understand their correlation. They can be seen in Figure 5.1.
The final step was to compare the efficiencies of the two decays by dividing them, as seen in Table 5.2. It was found that there is a significant difference in the TOS trigger conditions while they are in agreement for the TIS trigger condition.
This can be mostly traced back to different correlations in the different variables for the TIS and TOS condition. To understand exactly what the differences are and how they are to be understood, further variables need to be analysed. This means that future work will show us the exact differences in this regard, because at the moment, it is not possible to say more in this regard.

Chapter 7

Appendix

This chapter contains all of the criteria for each cut made during the work. The criteria TIS, TOS, and TISTOS appear in the first three lines.

- trigger:

$$
\begin{aligned}
&((((L1\_L0ElectronDecision\_TOS == 1)| \\
&(L\_L0ElectronDecision\_TOS == 1)) \\
&(B\_L0Global\_TIS == 1)) \\
&\&((B\_Hlt1TrackMVADecision\_TOS == 1)| \\
&(B\_Hlt1TwoTrackMVADecision\_TOS == 1))\& \\
&((B\_Hlt2Topo2BodyDecision\_TOS == 1)| \\
&(B\_Hlt2Topo3BodyDecision\_TOS == 1)| \\
&(B\_Hlt2Topo4BodyDecision\_TOS == 1)| \\
&(B\_Hlt2TopoE2BodyDecision\_TOS == 1)| \\
&(B\_Hlt2TopoE3BodyDecision\_TOS == 1)| \\
&(B\_Hlt2TopoE4BodyDecision\_TOS == 1)| \\
&(B\_Hlt2TopoEE2BodyDecision\_TOS == 1)| \\
&(B\_Hlt2TopoEE3BodyDecision\_TOS == 1)| \\
&(B\_Hlt2TopoEE4BodyDecision\_TOS == 1))
\end{aligned}
$$

- TISTOS:

$$
\begin{aligned}
&((((L1\_L0ElectronDecision\_TOS == 1)| \\
&(L\_L0ElectronDecision\_TOS == 1)))| \\
&(B\_L0Global\_TIS == 1))
\end{aligned}
$$

- TOS:

$$((L1\_L0ElectronDecision\_TOS == 1)| \\ (L2\_L0ElectronDecision\_TOS == 1))$$

- TIS:

$$((B\_L0Global\_TIS == 1))$$

Bibliography

[1] CERN. The large hadron collider. *journal*, 22 Mar 2021. URL https://arxiv.org/abs/2103.11769.

[2] CERN. Supdated measurement of r_k at lhcb. *journal*, 23 Mar 2021. URL https://arxiv.org/abs/2105.10303.

[3] CERN. Search for new physics with *bßsll* decays @ lhcb. *journal*, 23 Mar 2021. URL https://indico.cern.ch/event/572149/contributions/2449186/attachments/1445715/2227088/RKstar-LHCb.pdf.

[4] CERN. $k^*(892)$ mass. *journal*, 23 Mar 2021. URL https://pdg.lbl.gov/2013/listings/rpp2013-list-K-star-892.pdf.

[5] CERN. The large hadron collider. *journal*, 2000. URL https://home.cern/science/accelerators/large-hadron-collider.

[6] CERN. The lhc sees its first circulating beam. *journal*, Sept 2008. URL https://cerncourier.com/a/the-lhc-sees-its-first-circulating-beam/.

[7] CERN. The lhcb detector. *Journal*, 2008. URL http://lhcb-public.web.cern.ch/en/Detector/Detector-en.html.

[8] Xavier Vidal and Ramon Manzano. High vacuum. *journal*, 2000. URL https://www.lhc-closer.es/taking_a_closer_look_at_lhc/0.high_vacuum.

[9] The ATLAS Collaboration et al. The ATLAS experiment at the CERN large hadron collider. *Journal of Instrumentation*, 2008. URL http://hedberg.web.cern.ch/hedberg/home/atlas/atlas.html.

[10] CERN. Higgs boson. *journal*, 2000. URL https://home.cern/science/physics/higgs-boson.

[11] The CMS Collaboration et al. The CMS experiment at the CERN LHC. *Journal*, 2008. URL http://homepage.physics.uiowa.edu/~jnachtma/CMS11.html.

[12] CERN. CERN CMS. *journal*, 2000. URL https://home.cern/science/experiments/cms.

[13] Florido Paganelli. The ALICE experiment at the CERN LHC. *Journal*, 2021. URL https://www.particlephysics.physics.lu.se/research/alice/.

[14] CERN. CERN ALICE. *journal*, 2000. URL https://home.cern/science/experiments/alice.

[15] The LHCb Collaboration et al. The LHCb detector at the LHC. *Journal of Instrumentation*, 3(08):S08005–S08005, aug 2008. doi: 10.1088/1748-0221/3/08/s08005. URL https://doi.org/10.1088/1748-0221/3/08/s08005.

[16] CERN. CERN LHCb. *journal*, 2000. URL https://home.cern/science/experiments/lhcb.

[17] S. Mrenna T. Sj ostrand and P. Skands. A brief introduction to pythia 8.1. *Comput. Phys. Commun. 178*, 2008. URL https://arxiv.org/pdf/0710.3820.pdf.

[18] D. J. Lange. The evtgen particle decay simulation package. *Nucl. Instrum. Meth. A462 (2001) 152*, 2001. URL https://www.sciencedirect.com/science/article/pii/S0168900201000894?via%3Dihub.

[19] I. Belyaev. Handling of the generation of primary events in gauss, the lhcb simulation framework. *J. Phys. Conf. Ser. 331*, 2011. URL https://iopscience.iop.org/article/10.1088/1742-6596/331/3/032047/pdf.